Postprint

This is the accepted version of a paper published in *Journal of Physical Chemistry B*. This paper has been peer-reviewed but does not include the final publisher proof-corrections or journal pagination.

Permanent link to this version:
http://urn.kb.se/resolve?urn=urn:nbn:se:su:diva-148998

Conformational Dynamics and Exchange Kinetics of *N*-Formyl and *N*-Acetyl Groups Substituting 3-Amino-3,6-Dideoxy-α-D-Galactopyranose, a Sugar Found in Bacterial O-Antigen Polysaccharides

Olof Engström, Hani Mobarak, Jonas Ståhle and Göran Widmalm*

Department of Organic Chemistry, Arrhenius Laboratory, Stockholm University, SE-106 91 Stockholm, Sweden.

Email address of corresponding author: goran.widmalm@su.se

ABSTRACT

Three dimensional shape and conformation of carbohydrates are important factors in molecular recognition events and the *N*-acetyl group of a monosaccharide residue can function as a conformational gatekeeper whereby it influences the overall shape of the oligosaccharide. NMR spectroscopy and quantum mechanics (QM) calculations are used herein to investigate both the conformational preferences and the dynamic behavior of *N*-acetyl and *N*-formyl substituents of 3-amino-3,6-dideoxy-α-D-galactopyranose, a sugar and substitution patterns found in bacterial O-antigen polysaccharides. QM calculations suggest that the amide oxygen can be involved in hydrogen bonding with the axial OH4 group primarily but also with the equatorial OH2 group. However, an NMR *J* coupling analysis indicates that the θ_1 torsion angle, adjacent to the sugar ring, prefers an *ap* conformation where conformations $< 180°$ also are accessible, but does not allow for intramolecular hydrogen bonding. In the formyl-substituted compound ${}^4J_{\text{HH}}$ coupling constants to the *exo*-cyclic group were detected and analyzed. A van't Hoff analysis revealed that the *trans* conformation at the amide bond is favored by $\Delta G° \approx -0.8$ kcal·mol^{-1} in the formyl-containing compound and with $\Delta G° \approx -2.5$ kcal·mol^{-1} when the *N*-acetyl group is the substituent. In both cases the enthalpic term dominates to the free energy, irrespective of water or DMSO as solvent, with only a small contribution from the entropic term. The *cis–trans* isomerization of the θ_2 torsion angle, centered at the amide bond, was also investigated by employing ^{1}H NMR lineshape analysis and ^{13}C NMR saturation transfer experiments. The extracted transition rate constants were utilized to calculate transition energy barriers that were found to be about 20 kcal·mol^{-1} in both DMSO-d_6 and D$_2$O. Enthalpy had a higher contribution to the energy barriers in DMSO-d_6 compared to in D$_2$O, where entropy compensated for the loss of enthalpy.

INTRODUCTION

Molecular properties defined by shape and charge form the basis of interaction and recognition processes. In molecules certain parts make up a framework or core onto which functional groups are appended thereby giving the molecules specific characteristics such as hydrogen bonding abilities or the possibility to participate in π-stacking interactions as well as complementary hydrophobic interactions. The different substituents cover a wide range of properties present in e.g. halogens, amines, amides, hydroxyl, carboxyl, ester, phosphate and sulfate groups. In carbohydrates, a sugar residue having an amino group in lieu of a hydroxyl group is one of the most common alterations to a monosaccharide entity.

The amino group of sugar components in polysaccharides is sometimes non-substituted, as in the capsular polysaccharide from *S. pneumoniae* type 1[1] and the O-polysaccharide from *S. sonnei*,[2] but most often it is substituted as an amide where the carbonyl group with its alkyl chain or functionalized alkyl chain is of different length and chirality. The amino groups have been described to be acylated e.g. as *N*-formyl groups in the O-antigen polysaccharides from *Bordetella bronciseptica* Bp512[3] and *Brucella suis* serovar 2,[4] as *N*-acetyl groups in *Proteus penneri* strain 26[5] and *E. coli* O74,[6] substituted with 3-deoxy-L-*glycero*-tetronic acid in *V. cholerae* O1[7] and with 3-hydroxybutanoic acid in *Pseudomonas aeruginosa* IID 1001.[8]

The conformation of the *N*-acyl group in *N*-acetyl-D-glucosamine, which is a major constituent in glycosaminoglycans, has predominantly a *trans* orientation of the torsion angle $O=C-N-H_N$ with respect to the amide bond[9,10] whereas in *N*-formyl-perosamine, which constitutes the sugar residue in *Brucella* O-antigen homopolymers,[11] a conspicuous equilibrium exists where both the s-*cis* (*Z*) and s-*trans* (*E*) conformations are populated to a significant extent, with the former conformation being favored.[12] Molecular dynamics simulations have shown that conformational transitions at the $H2-C2-N-H_N$ torsion angle of *N*-acetyl-D-glucosamine as part of oligosaccharides can influence conformational space available at glycosidic torsion angles not related to the amino sugar per se, a finding that may have biological significance.[13,14,15] In methyl 2-acylamido-2-deoxy-D-glucopyranosides *N*-formylation also leads to significant populations of both the *cis* and *trans* conformations,[10] where the latter predominates. Most interestingly, ^{13}C isotopic labeling in the *N*-acetyl group facilitated detection of the minor *cis* conformer present to only 2%.

We have previously synthesized *N*-acyl substituted derivatives of methyl 3-amino-3,6-dideoxy-α-D-galactopyranoside, as a model for the sugar D-Fuc*p*3N present in several bacterial O-antigen polysaccharides,[16] and found that the *N*-formyl group populated two readily observed conformational states whereas the *N*-acetyl derivative was indicated to have a single (major or exclusive) state at the

amide bond.[17] Herein we extend the analysis to conformation and dynamics of methyl 3,6-dideoxy-3-formamido-α-D-galactopyranoside (**1**) and methyl 3-acetamido-3,6-dideoxy-α-D-galactopyranoside (**2**) by utilizing in addition to the natural abundance compounds also site-specifically labeled derivatives, viz., 3,6-dideoxy-3-[1-^{13}C]formamido-α-D-galactopyranoside (**1**$_{C1'}$), 3-[1-^{13}C]acetamido-3,6-dideoxy-α-D-galactopyranoside (**2**$_{C1'}$) and 3-[2-^{13}C]acetamido-3,6-dideoxy-α-D-galactopyranoside (**2**$_{C2'}$) (Figure 1) synthesized to this end.
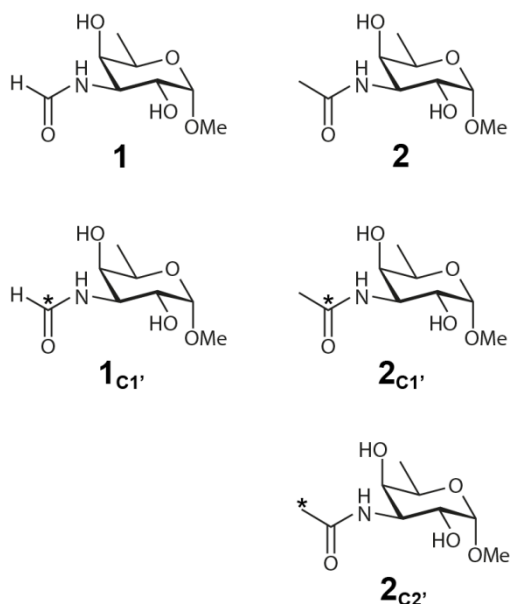
Figure 1. Structures of the compounds synthetized and investigated in this study; natural abundance α-D-Fuc*p*3NFo-OMe (**1**) and α-D-Fuc*p*3NAc-OMe (**2**) and the related site-specifically ^{13}C isotopically labeled compounds α-D-Fuc*p*3N[1'-^{13}C]Fo-OMe (**1**$_{C1'}$), α-D-Fuc*p*3N[1'-^{13}C]Ac-OMe (**2**$_{C1'}$) and α-D-Fuc*p*3N[2'-^{13}C]Ac-OMe (**2**$_{C2'}$). An asterisk marks labeling position.

EXPERIMENTAL SECTION

Synthesis. The compounds used for the NMR experiments were synthetized as described elsewhere[17] except for the amidation of compounds **1**$_{C1'}$, **2**$_{C1'}$ and **2**$_{C2'}$ that were made by a different procedure.[18] Methyl 3-amino-2,4-di-*O*-benzyl-3,6-dideoxy-α-D-galactopyranoside[17] was dissolved in a microwave vial with DCM, the formic acid (^{13}C-labeled at C1, 1.1 eq) or acetic acid (either ^{13}C-labeled at C1 or at C2, 1.1 eq), 2-chloro-4,6-dimethoxy-1,3,5-triazine (1.2 eq.) and 4-methylmorpholine (1.2 eq.). A catalytic amount of DMAP was added and the vial was placed in a microwave synthesizer (Biotage® Initiator Classic, Biotage, Uppsala, Sweden) at 40 °C where irradiation was carried out at 2.45 GHz for 15 min. The reaction mixture was diluted with DCM, washed with HCl, sodium bicarbonate and brine. The solvent was evaporated and the crude material was dissolved in EtOH. Pd-C was added and the protected monosaccharide was subjected to hydrogenolysis overnight. The reaction mixture was filtered through Celite, the solvent was

3

evaporated and the crude material was purified using a Sep-Pak® C-18 cartridge using water as eluent. The fractions containing the product were collected and freeze-dried to obtain the products as white solids in yields of 73% to 75%. NMR data in full agreement with those previously published;[17] additionally detected ^{13}C NMR resonance of minor conformer in labeled compound $\mathbf{2}_{C1'}$ (D$_2$O): 177.6 ppm (C=O). ESIMS: [M+Na]$^+$ m/z calcd for $\mathbf{1}_{C1'}$ C$_7$^{13}CH$_{15}$NO$_5$Na 229.0876, found 229.0865, calcd for $\mathbf{2}_{C1'}$ C$_8$^{13}CH$_{17}$NO$_5$Na 243.1032, found 243.1033, calcd for $\mathbf{2}_{C2'}$ C$_8$^{13}CH$_{17}$NO$_5$Na 243.1032, found 243.1026. The ^{13}C labeling was confirmed by inspection of 1D ^{13}C NMR spectra. NMR samples of the five compounds were prepared in both D$_2$O and DMSO-d_6, after freeze drying from D$_2$O, where applicable.

Methyl 3-formamido-3,6-dideoxy-α-D-galactopyranoside (1). Major ^{1}H NMR (500 MHz, 25 °C, DMSO-d_6): δ 1.06 (d, $J_{H5,H6}$ 6.6 Hz, 2.4H, H-6), 3.28 (s, 2.4H, OMe), 3.46 (dd, $J_{H3,H4}$ 3.1 Hz, $J_{H4,H5}$ 1.3 Hz, 0.8H, H-4), 3.60 (dd, $J_{H1,H2}$ 3.6 Hz, $J_{H2,H3}$ 11.2 Hz, 0.8H, H-2), 3.76 (dd, $J_{H4,H5}$ 1.3 Hz, $J_{H5,H6}$ 6.6 Hz, 0.8H, H-5), 4.00 (dddd, $J_{H2,H3}$ 11.2 Hz, $J_{H3,H4}$ 3.1 Hz, $J_{H3,NH}$ 8.4 Hz, $J_{H3,HFo}$ −0.8 Hz, 0.8H, H-3), 4.41 (br, 0.8H, OH2), 4.51 (d, $J_{H1,H2}$ 3.6 Hz, 0.8H, H-1), 4.90 (br, 0.8H, OH4), 7.82 (dd, $J_{H3,NH}$ 8.4 Hz, $J_{NH,HFo}$ 1.8 Hz, 0.8H, NH), 8.02 (dd, $J_{H3,HFo}$ −0.8 Hz, $J_{NH,HFo}$ 1.8 Hz, 0.8H, H-Fo). ^{13}C NMR (125 MHz, 25 °C, DMSO-d_6): δ 16.4 (C-6), 49.8 (C-3), 54.6 (OMe), 65.6 (C-2), 65.8 (C-5), 69.8 (C-4), 99.7 (C-1), 161.2 (CO). Minor ^{1}H NMR (500 MHz, 25 °C, DMSO-d_6): δ 1.07 (d, $J_{H5,H6}$ 6.8 Hz, 0.6H, H-6), 3.28 (s, 0.6H, OMe), 3.47 (dddd, $J_{H2,H3}$ 10.1 Hz, $J_{H3,H4}$ 2.7 Hz, $J_{H3,NH}$ 9.7 Hz, $J_{H3,HFo}$ −0.3 Hz, 0.2H, H-3), 3.49 (dd, $J_{H3,H4}$ 2.7 Hz, $J_{H4,H5}$ 1.3 Hz, 0.2H, H-4), 3.51 (dd, $J_{H1,H2}$ 3.6 Hz, $J_{H2,H3}$ 10.1 Hz, 0.2H, H-2), 3.78 (dd, $J_{H4,H5}$ 1.3 Hz, $J_{H5,H6}$ 6.8 Hz, 0.2H, H-5), 4.53 (d, $J_{H1,H2}$ 3.6 Hz, 0.2H, H-1), 4.73 (br, 0.2H, OH2), 4.96 (br, 0.2H, OH4), 6.89 (dd, $J_{H3,NH}$ 9.7 Hz, $J_{NH,HFo}$ 11.7 Hz, 0.2H, NH), 7.95 (dd, $J_{NH,HFo}$ 11.7 Hz, $J_{H3,HFo}$ −0.3 Hz, 0.2H, H-Fo). ^{13}C NMR (125 MHz, 25 °C, DMSO-d_6): δ 16.3 (C-6), 53.6 (C-3), 54.5 (OMe), 65.9 (C-2), 66.0 (C-5), 71.0 (C-4), 99.6 (C-1), 164.5 (CO).

Methyl 3-acetamido-3,6-dideoxy-α-D-galactopyranoside (2). Major ^{1}H NMR (500 MHz, 25 °C, DMSO-d_6): δ 1.05 (d, $J_{H5,H6}$ 6.5 Hz, 3H, H-6), 1.83 (s, 3H, Ac), 3.27 (s, 3H, OMe), 3.46 (dd, $J_{H3,H4}$ 3.0 Hz, $J_{H4,H5}$ 0.8 Hz, 1H, H-4), 3.62 (dd, $J_{H1,H2}$ 3.6 Hz, $J_{H2,H3}$ 11.2 Hz, 1H, H-2), 3.75 (dd, $J_{H4,H5}$ 0.8 Hz, $J_{H5,H6}$ 6.5 Hz, 1H, H-5), 3.92 (ddd, $J_{H2,H3}$ 11.2 Hz, $J_{H3,H4}$ 3.0 Hz, $J_{H3,NH}$ 8.1 Hz, 1H, H-3), 4.35 (br, 1H, OH-2), 4.50 (d, $J_{H1,H2}$ 3.6 Hz, 1H, H-1), 4.83 (br, 1H, OH-4), 7.58 (d, $J_{H3,NH}$ 8.1 Hz, 1H, NH). ^{13}C NMR (125 MHz, 25 °C, DMSO-d_6): δ 16.6 (C-6), 23.0 (Ac), 51.5 (C-3), 54.8 (OMe), 65.8 (C-2), 66.0 (C-5), 70.0 (C-4), 99.9 (C-1), 170.0 (CO); additionally detected ^{13}C NMR resonance of minor conformer in labeled compound $\mathbf{2}_{C1'}$: 171.3 ppm (C=O).

Measurements of NMR *J* coupling constants. Scalar spin-spin couplings were extracted from experiments performed at 25 °C on a 600 MHz NMR spectrometer equipped with either a 5 mm

inverse-detection triple-resonance probe or a 5 mm broadband probe and on a 500 MHz NMR spectrometer equipped with a cryoprobe. Homonuclear ^{1}H J coupling constants were fitted from 1D ^{1}H NMR spectra of **1** and **2** in DMSO-d_6 (acquired with acquisition times of 2.0 s or 2.7 s, respectively, and processed with a Lorentzian-Gaussian window function (lb = −2 Hz or −1 Hz and gb = 0.25 or 0.3, respectively) by employing the NMR spin simulation software PERCH.[19] 1D ^{13}C spectra of **1**$_{C1'}$, **2**$_{C1'}$ and **2**$_{C2'}$ in D$_2$O and in DMSO-d_6 (with acquisition times ranging between 1.4 s to 1.7 s and processed with resolution enhancement by applying Lorentzian-Gaussian window functions (−1 Hz to −3 Hz and gb = 0.3 or 0.7, respectively), prior Fourier transformation) were used in the extraction of vicinal homonuclear ^{13}C J couplings by employing the J-doubling method.[20,21] J-HMBC experiments[22] were recorded with 128 scans and 16 dummy scans. The carrier was set at 5 ppm and 90 ppm with spectral widths of 10 ppm and 180 ppm; 16k and 256 data points were acquired in the direct and indirect dimensions, respectively. A sine and a sine-squared window function were added in the F_2 and F_1 dimensions, respectively. The indirect dimension was zero-filled to 2k data-points and linear prediction was applied prior to Fourier transformation and subsequent presentation in magnitude mode. Heteronuclear ^{1}H,^{13}C J couplings were measured from the cross-peak splitting in the indirect dimension of spectra with scaling factors varying between 20 and 60.

^{1}H,^{1}H-NOESY NMR spectroscopy. A 2D ^{1}H,^{1}H-NOESY experiment with a zero-quantum suppression filter[23] was performed at 25 °C using a 500 MHz NMR spectrometer equipped with a cryoprobe on a sample containing **1** in DMSO-d_6. The spectrum was recorded with 32k and 256 data points in the F_2 and F_1 dimensions, respectively, using an inter-scan delay of 3 s and a mixing time (τ_{mix}) of 200 ms. The spectral width was set to 10 ppm and the carrier was set at 4.76 ppm. Cosine-squared functions were applied in each dimension and a linear prediction with 120 coefficients and 256 data points was applied in F_1, which then was zero-filled to 1k data points prior Fourier transformation. Cross-relaxation rates (σ_{ij}) were calculated as ($I_j/[-I_i \cdot \tau_{\mathrm{mix}}]$) with I_j being the volume of the cross-peak and I_i being the volume of the corresponding diagonal peak.[24] Effective proton-proton distances were calculated as $r_{ij} = r_{\mathrm{ref}} \left(\sigma_{\mathrm{ref}} / \sigma_{ij} \right)^{1/6}$, where the reference distance was obtained from a quantum mechanical geometry optimized model (vide infra).

^{13}C NMR spin-relaxation experiments. The ^{13}C fast T_1 inversion-recovery experiments[25] and saturation-recovery (SR) experiments were performed on a 600 MHz NMR spectrometer equipped with a 5 mm broadband probe pre-calibrated to the desired temperature using a thermocouple. NMR spectra were recorded on **1**$_{C1'}$ and **2**$_{C1'}$ in D$_2$O and in DMSO-d_6, using 58k data points and spectral widths of 300 ppm. An exponential line-broadening window function of 1 Hz was applied prior Fourier transformation. For the fast T_1 inversion-recovery experiments the carrier was set to 162 ppm

employing 16 or 32 scans. At least two dummy scans were used and inter-scan delays of 8 – 16 s were applied. T_1 relaxation times were fitted to the peak intensities of eight experiments with varying mixing times from 1 ms to 10 s employing the fitting routine available in Topspin 3.1 (Bruker). The ^{13}C saturation-transfer (ST) experiments[26] were performed by stepwise setting the carrier on the C1' resonances of $1_{C1'}^{minor}$ and $2_{C1'}^{minor}$, and applying a continuous wave irradiation of 100 Hz and of varying length. Spectra were acquired using 16 scans, at least two additional dummy scans and inter-scan delays of $> 10 \times T_1$. Experiments were performed in duplicates with shuffled mixing times ranging between 0.1 and 5 s and appearing in opposite order in each duplicate. The exchange rates and $M_z(0)$ were fitted to peak intensities of the corresponding resonance in the alternative conformer based on Equation 11 (vide infra) employing an in-house MATLAB (MathWorks) script.

^{1}H NMR Lineshape analysis. 1D ^{1}H NMR spectra of **1** in DMSO-d_6 acquired on a 600 MHz NMR spectrometer equipped with a 5 mm inverse-detection triple-resonance probe, where the temperature had been pre-calibrated using a thermocouple, were used in the lineshape analysis employing the spin simulation DNMR tool featured in Topspin 3.1 (Bruker). Spin systems of H1, H2, H5, Me6 or H_{Fo} and related coupled spins were utilized in the fit; the apparent spectral line broadening factor (lb), used as an input parameter in the fitting procedure, was estimated from the solvent quintet.

***J*-based conformational analysis.** The conformational relationship of vicinal *J* couplings related to θ_1 and θ_2 torsions of the α- and β-anomeric forms of D-Glc*p*NAc and D-All*p*NAc were investigated by Hu et al.[27] employing density functional theory (DFT) calculations and the authors presented two (depending on the conformation of the other θ torsion) Karplus-type equations for vicinal spin-pairs of both torsions; the molecular resemblance between α-D-Glc*p*NAc and **2** as well as **1** makes these equations appropriate for this study. The relationships associated to the θ_1 torsion angle in **1** and **2** are described in Equations 1 – 5 where *a* and *b* notations relate to the conformation of θ_2 which is either *cis* or *trans*, respectively.

$$^3J_{C2,C1'} = 1.12 - 0.97\cos(\theta_1 + 60°) + 1.35\cos(2(\theta_1 + 60°)) - 0.16\sin(\theta_1 + 60°) + 0.04\sin(2(\theta_1 + 60°)) \qquad (1a)$$

$$^3J_{C2,C1'} = 1.11 - 0.87\cos(\theta_1 + 60°) + 1.15\cos(2(\theta_1 + 60°)) - 0.09\sin(\theta_1 + 60°) + 0.08\sin(2(\theta_1 + 60°)) \qquad (1b)$$

$$^3J_{C4,C1'} = 1.12 - 0.97\cos(\theta_1 - 60°) + 1.35\cos(2(\theta_1 - 60°)) - 0.16\sin(\theta_1 - 60°) + 0.04\sin(2(\theta_1 - 60°)) \qquad (2a)$$

$$^3J_{C4,C1'} = 1.11 - 0.87\cos(\theta_1 - 60°) + 1.15\cos(2(\theta_1 - 60°)) - 0.09\sin(\theta_1 - 60°) + 0.08\sin(2(\theta_1 - 60°)) \qquad (2b)$$

$$^3J_{H3,C1'} = 3.19 - 2.12\cos(\theta_1 + 180°) + 3.3\cos(2(\theta_1 + 180°)) - 0.02\sin(\theta_1 + 180°) +$$
$$0.06\sin(2(\theta_1 + 180°)) \qquad\qquad (3a)$$

$$^3J_{H3,C1'} = 3.11 - 2.02\cos(\theta_1 + 180°) + 2.88\cos(2(\theta_1 + 180°)) - 0.04\sin(\theta_1 + 180°) +$$
$$0.05\sin(2(\theta_1 + 180°)) \qquad\qquad (3b)$$

$$^3J_{C2,HN} = 3.14 - 0.78\cos(\theta_1 - 120°) + 3.47\cos(2(\theta_1 - 120°)) - 0.16\sin(\theta_1 - 120°) +$$
$$0.37\sin(2(\theta_1 - 120°)) \qquad\qquad (4a)$$

$$^3J_{C2,HN} = 2.57 - 0.61\cos(\theta_1 - 120°) + 2.92\cos(2(\theta_1 - 120°)) - 0.09\sin(\theta_1 - 120°) +$$
$$0.27\sin(2(\theta_1 - 120°)) \qquad\qquad (4b)$$

$$^3J_{H3,HN} = 5.99 - 0.59\cos\theta_1 + 6.11\cos(2\theta_1) + 0.10\sin\theta_1 + 0.12\sin(2\theta_1) \qquad\qquad (5a)$$

$$^3J_{H3,HN} = 5.08 - 0.83\cos\theta_1 + 5.02\cos(2\theta_1) + 0.03\sin\theta_1 + 0.06\sin(2\theta_1) \qquad\qquad (5b)$$

The θ_2 torsion of **2** can be described by Equation 6, as well as by Equations 7a and 7b where a and b notations relate to the conformation of θ_1, which is either *sp* or *ap*, respectively.

$$^3J_{NH,C2'} = 1.62 - 2.59\cos(\theta_2 + 180°) + 1.29\cos(2(\theta_2 + 180°)) + 0.67\cos(3(\theta_2 + 180°)) +$$
$$0.02\sin(\theta_2 + 180°) - 0.02\sin(2(\theta_2 + 180°)) + 0.003\sin(3(\theta_2 + 180°)) \qquad\qquad (6)$$

$$^3J_{C3,C2'} = 0.84 - 2.03\cos\theta_2 + 0.60\cos(2\theta_2) + 0.13\cos(3\theta_2) + 0.04\sin\theta_2 - 0.02\sin(2\theta_2) -$$
$$0.002\sin(3\theta_2) \qquad\qquad (7a)$$

$$^3J_{C3,C2'} = 0.39 - 1.03\cos\theta_2 + 0.36\cos(2\theta_2) + 0.25\cos(3\theta_2) - 0.01\sin\theta_2 + 0.02\sin(2\theta_2) -$$
$$0.004\sin(3\theta_2) \qquad\qquad (7b)$$

Karplus equations involving H_{Fo} are less well developed for the current spin system. For the $^3J_{HN,HFo}$ coupling the H_N-$H_{C\alpha}$ relationship derived for proteins[28] can be employed as an approximation (Equation 8).

$$^3J_{NH,HFo} = 6.7\cos(2(\theta_2 + 180°)) + 1.3\cos(\theta_2 + 180°) + 1.5 \qquad\qquad (8)$$

Equation 9, applied for the $^3J_{C3,HFo}$ coupling, is also an approximation as it is originally derived for the CO-$H_{C\alpha}$ relationship in proteins.[29]

$$^3J_{C3,HFo} = 3.96\cos(2\theta_2) - 1.83\cos\theta_2 + 0.81 \qquad\qquad (9)$$

RMSD between calculated values and experimental data were computed for different torsion angles. Three-state models describing the dynamics around θ_1 were made based on the results from potential energy calculations and J coupling analysis. Populations were fitted by minimizing the RMSD

between experimentally determined J couplings and those calculated using Equations 1b – 9 implemented in Excel (Microsoft).

Geometry Optimization and Energy Calculations. Geometry optimizations were performed by scanning the θ_1 (H3-C3-N-H$_N$) and θ_2 (H$_N$-N-C1'-O) torsion angles using 15° increments covering 360°. The first set of calculations were carried out on **1**, which had only the scanned torsions (θ_1 and θ_2) and the linear bend, C3-H$_N$-C1'-N, centered on the amide nitrogen computed using the command *frozen*, thus constraining the nitrogen to an sp^2 geometry. For the second set, carried out for both **1** and **2**, the dihedrals Hn-Cn-On-HOn for the hydroxyl groups at positions 2 and 4 were restrained to −50° and −30° as well, to prevent intramolecular hydrogen bonding. The scans were performed with the *Gaussian09RevD.01*[30] package using the B3LYP functional and the 6-31G* basis set. For all sets the effect of solvent was considered by using a conductor-like polarizable continuum model (CPCM)[41,42] specifying either H$_2$O or DMSO.

Calculation of NMR J coupling constants. NMR parameters for scalar spin-spin coupling constants were calculated for α-D-Fuc$p$3NF$_0$-OMe from geometries optimized for DMSO scanning θ_1 (H3-C3-N-H$_N$) using 2° increments, using the B3LYP functional and the 6-31G* basis set. The same constrains were used as for the second set of the geometry and energy calculation, with the addition of also restricting θ_2 to either an anti- or syn-conformation, thus forming two sets. Subsequently, NMR parameters were calculated using the Gauge-Independent Atomic Orbital method (GIAO)[43,44] and DFT with the B3LYP functional[45] and the basis set 6-311+G(d,p). The *mixed* keyword was invoked to calculate the spin-spin coupling with a two-step method, viz., first the Fermi Contact term using an extended basis set and then the remaining three terms are calculated using an unmodified basis set.[46]

RESULTS AND DISCUSSION

QM energy calculations. The change in potential energy in compounds **1** and **2** for different conformations around the θ_1 and θ_2 torsion angles, defined as H3-C3-N-H$_N$ and O=C1'-N-H$_N$, respectively (Figure 2), were investigated by QM energy calculations. To examine the effects of intramolecular hydrogen bonding (HB) between the carbonyl oxygen and the hydroxyl groups OH2 or OH4, two sets of calculations were carried out. In one of them the hydroxyl groups were restrained pointing away from the amide side-chain, thus preventing the possibility of hydrogen bonding. In all calculations, high energy conformers are related to θ_2 clinal arrangements, which are ~30 kcal·mol^{-1} higher in energy than corresponding *cis* and *trans* conformations (Figure 3). These values are higher than reported for amides in general, which could arise from the fact that the nitrogen atom was

8

constrained in an sp^2-geometry in the calculations whereas in the transition state it adopts a more sp^3-like character.[37]
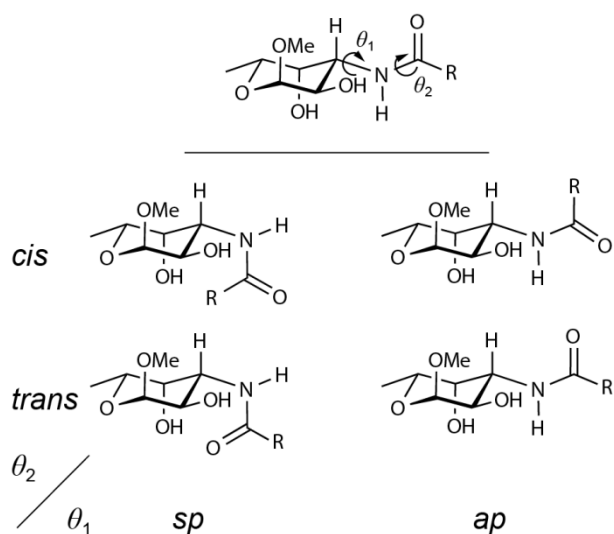
Figure 2. The two torsion angles θ_1 (defined as H3-C3-N-H$_N$) and θ_2 (defined as O=C1'-N-H$_N$) describing the amide side-chain conformation (top) and the four canonical conformations of α-D-Fuc$p$3NH(CO)R-OMe (**1** R = H; **2** R = Me) (bottom).
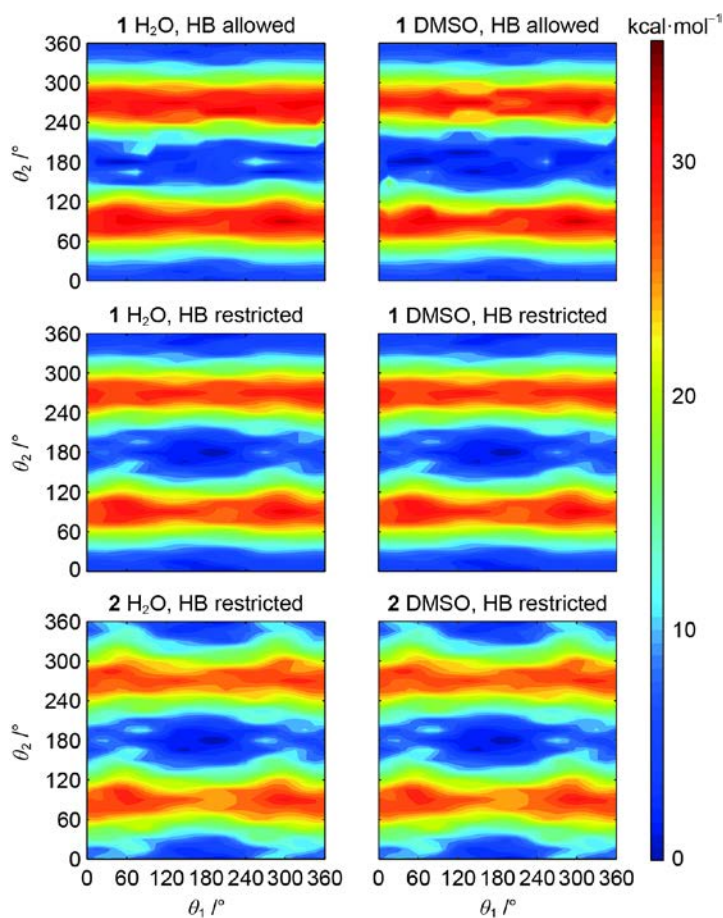
Figure 3. QM calculated energy landscapes as a function of θ_2 vs. θ_1, solvent (H$_2$O, left column; DMSO, right column) and hydrogen bonding between hydroxyl groups of the sugar residue and the carbonyl oxygen of the amide substituent.

The potential energies that resulted from calculations in which HB possibilities were limited, were very similar when comparing the results of **1** in different solvent models. Energy minima are observed for *ap,trans* (θ_1, θ_2; 195°, 180°) conformations primarily but also for *+ac,cis* (θ_1, θ_2; 135°, 345°) which is 1.7 kcal·mol^{-1} higher in energy. When HB was allowed in the calculations, the energy minima of **1** were shifted in both solvents to $\theta_1 = 60°$ and $\theta_2 = 180°$, thus permitting a HB between the carbonyl oxygen and the hydroxyl proton of OH4. The potential energy well of the θ_2 torsion angle is significantly broader in DMSO than in H$_2$O and an additional minimum is also observed at $\theta_1 = 285°$ and $\theta_2 = 180°$, a conformation allowing a HB in a similar fashion but instead between the carbonyl oxygen and the hydroxyl proton of OH2. Restricting the HB possibilities results in lower energy barriers for the *cis–trans* isomerization at θ_2 due to higher energy of the global minima in these calculations.

Calculations of the potential energy landscape of compound **2** were carried out only with restriction of HB. Energy minima were similar to the ones found for compound **1** ($\theta_1 = 195°$, $\theta_2 = 180°$ and ($\theta_1 = 135°$, $\theta_2 = 345°$); however, when the θ_2 torsion angle has the *cis* orientation the *sp* arrangement at θ_1 in **2** is not as favorable as in **1**, due to steric clashes of the methyl group with hydroxyl groups on the sugar ring. Also, the energy barriers are lower for the *N*-acetyl-containing compound **2** compared to those of the *N*-formyl-containing compound **1**.

NMR-based conformational analysis. From NMR spectra at room temperature both **1** and **2** appear to have two conformations each, which are in slow chemical exchange with a major/minor population ratio of ~4 in the former and ~80 in the latter. The conformations of the amide side-chains of both **1** and **2** at room temperature were investigated by employing a *J*-based analysis, focused on samples in DMSO-*d*$_6$ since the amide proton is not available in D$_2$O because of solvent deuterium exchange. Homonuclear proton-proton couplings were extracted from 1D ^{1}H NMR spectra of **1** and **2** employing the NMR spin-simulation software PERCH.[19] Homonuclear carbon couplings were measured utilizing the J-doubling method[20,21] on the peak separation of spin resonances (*viz.*, C2, C3 and C4) coupled to the ^{13}C isotopically labeled C1' or C2' in ^{13}C NMR spectra of **1**$_{C1'}$, **2**$_{C1'}$ and **2**$_{C2'}$. ^{1}H,^{13}C-Heteronuclear coupling constants were obtained by the J-HMBC experiment.[22] *J* couplings were measured for **1**^{major}, **1**^{minor} and **2**^{major}, but not for **2**^{minor} due to the low abundance of this conformer, and the results are presented in Table 1.

Table 1. *J* coupling constants (Hz) measured for **1** and **2** at 25 °C.

	Spin pair	DMSO-d_6			D$_2$O		
		1 *major*	**1** *minor*	**2** *major*	**1** *major*	**1** *minor*	**2** *major*
θ_1	C1'-C2	1.47	n.d.[a]	1.90	1.52	1.14	1.78
	C1'-C4	n.d.[a]	1.48	0.71	0.76	n.d.	0.76
	C1'-H3	2.69	4.99	3.53	3.12	5.59	3.37
	H$_N$-C2	n.d.	n.d.	3.16	-	-	-
	H$_N$-H3	8.38	9.67	8.07	-	-	-
θ_2	H$_N$-H$_{Fo}$/C2'	1.85	11.72	n.d.[a]	-	-	-
	C3-H$_{Fo}$/C2'	5.85	2.17	1.70	5.02	1.15	1.65
$^4J_{HH}$	H3-H$_{Fo}$	0.83	0.3	-	0.89	0.3	-

[a] Set to zero in RMSD calculations

n.d. = not determined

The magnitude of vicinal *J* couplings is dependent on the torsional angle between the coupled spins, a relationship that can be described by a Karplus-type of equation which depends on the atoms involved in the bond-network connecting the coupled spins. Theoretical *J* coupling constants (in absolute values since the signs of the *J* couplings are not known) based on Karplus-type relationships presented in the Experimental section were calculated as functions of θ_1 and θ_2 and the RMSD between theoretical and experimental values are presented in Figure 4.
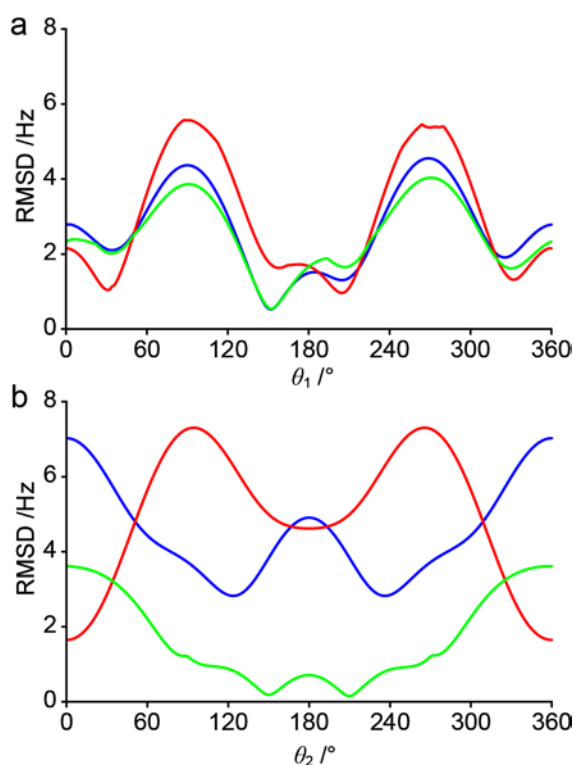
Figure 4. Minimization plots of experimental data in DMSO-d_6 (Table 1) and theoretical *J* couplings, calculated employing Karplus-type equations, for **1**^{major} (blue), **1**^{minor} (red) and **2**^{major} (green) for the θ_1 (a) and θ_2 (b) torsion angles.

Thus, $\mathbf{1}^{major}$ and $\mathbf{2}^{major}$ both occur in *trans* conformations with regard to θ_2 whereas $\mathbf{1}^{minor}$ adopts a *cis* conformation (Figure 4b). The assignment of $\mathbf{1}^{major}$ having the *trans* orientation at the θ_2 amide linkage and consequently $\mathbf{1}^{minor}$ as the *cis* conformation is fully consistent with those obtained for methyl 2-deoxy-2-formamido-α/β-D-glucopyranoside having $^3J_{HN,HFo} = 11.6$ Hz and $^3J_{HN,HFo} \approx 2$ Hz for the *cis* and *trans* conformations in DMSO-d_6, respectively.[10] In the minor conformation of $\mathbf{1}^{cis}$, $^3J_{HN,HFo} = 11.72$ Hz, i.e., the J coupling is large since the torsion angle H_N-N-C1'-H_{Fo} in this conformation is ~180° and in the major conformation of $\mathbf{1}^{trans}$, $^3J_{HN,HFo} = 1.85$ Hz, where the torsion angle is ~0°. The stereochemical assignment at the C1'-N bond of $\mathbf{1}^{cis}$ and $\mathbf{1}^{trans}$ is further supported by the ^1H T_1 relaxation times of the formyl proton being 4.5 s and 14.8 s at 600 MHz, 55 °C, in D_2O, respectively, i.e., differing by a factor of three, due to the spatial proximity to the ring proton H3 (cf. Figure 2, *ap,cis* conformation). This fully consistent with a previous observation for *N*-formyl-perosamine where the relaxation time of the formyl proton when present in the *cis* conformation was about three times shorter, than for the *trans* conformation, due to a corresponding stereochemical arrangement.[12]

However, for $\mathbf{1}^{trans}$ and $\mathbf{2}^{trans}$ the conformations appear to be shifted ±50° and ±30°, respectively, from an ideal 180° *trans* conformation. Even though amides have a planar structure they still allow some flexibility at θ_2 (±10°) without increasing the potential energy significantly.[37] Our calculations of the potential energy show that even though the energy well is quite flat and broad in the θ_2 dimension, shifts of > 30° from an idealized *trans* conformation are highly unlikely. The θ_2 torsion angles observed in the J coupling analysis, especially for $\mathbf{1}^{trans}$, could be caused by the choice of available Karplus equations, which are derived for proteins in the cases of $^3J_{HN,HFo}$ and $^3J_{C3,HFo}$.

Regarding the θ_1 torsion angle, both $\mathbf{1}^{trans}$ and $\mathbf{2}^{trans}$ have RMSD minima at 150° that correspond to an *ap* arrangement (RMSD = 0.55 and 0.57 Hz, respectively). These results are in agreement with a conformational survey of *N*-acetyl-D-glucosamine residues found in crystal structures of the RCSB PDB database (www.rcsb.org/pdb) revealing that the θ_1 torsion has its highest probability from 140° (+*anticlinal* conformation referred to as +*ac*) to 180° for these compounds.[10] A reason for this shift to the +*ac* conformation could be that for α-D-Glc*p*NAc, the axial orientation of the anomeric exocyclic oxygen reduces the steric clashes for the amide oxygen in this conformation. The same reasoning can be applied to $\mathbf{1}$ and $\mathbf{2}$ as the geometry around position 3 in this sugar (O4 axial and O2 equatorial) is related to position 2 of α-D-Glc*p*NAc (O1 axial and O3 equatorial), i.e., the amide group is tilted away from O2 towards H4 in the α-D-Fuc*p*3NAcyl-OMe compounds. The fact that the *N*-acetyl group in $\mathbf{2}$ is slightly tilted is fully consistent with results obtained from an NMR and circular dichroism spectroscopy study of human milk oligosaccharides, which, inter alia, contain a D-

GlcpNAc residue.[38] On the other hand, **1**^{cis} has three minima θ_1 = 30°, 205° and 330° (RMSD = 1.0 and 0.97 and 1.3 Hz, respectively) but not at θ_1 = 150°, possibly due to the fact that steric effects are less important as the amide oxygen is pointing towards the bulk solution for this conformer.

The preference of the *trans* over the *cis* conformation at the amide θ_2 torsion angle was investigated by analyzing ln K_{eq} vs. $1/T$, where T is the absolute temperature in Kelvin, in a van't Hoff plot[39] (Figure 5). By assuming that the ΔH of the reaction is temperature independent, ΔH and ΔS can be calculated by linear regression in which the negative slope and the y-intercept of the fitted line corresponds to ΔH and ΔS, respectively, both divided by the gas constant. The K_{eq} values at different temperatures were obtained for **1** from ^{1}H NMR spectra and for **2** from ^{13}C NMR spectra using the C1'-isotopically labeled compound (Table 2). The thermodynamic parameters calculated from this analysis are compiled in Table 3. The entropic contribution to the free energy is small in all cases and the latter is governed largely by the enthalpic term. The influence of solvent, one with both accepting and donating hydrogen bonding abilities and the other having only acting as an acceptor, on the conformational equilibrium for both **1** and **2** is negligible.
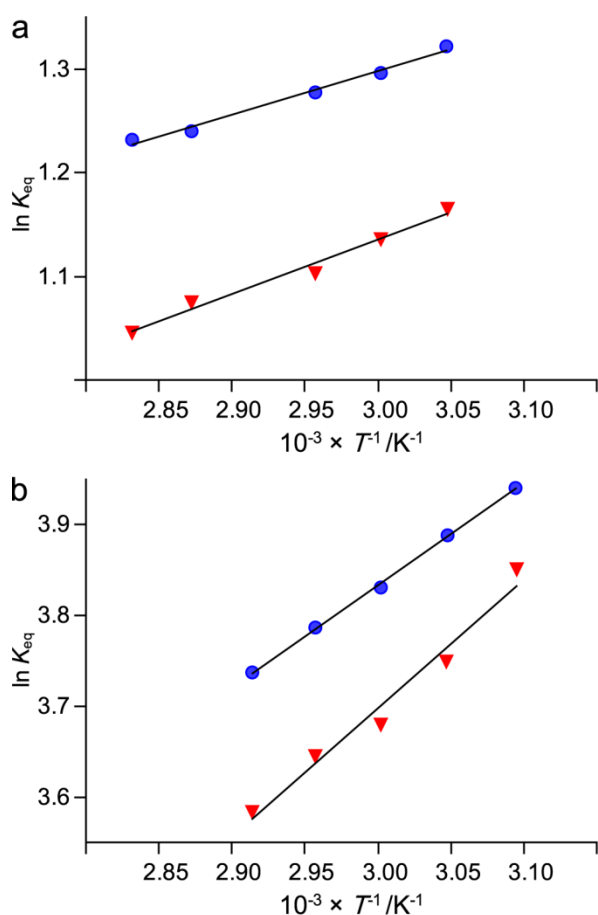
Figure 5. van't Hoff plots for compound **1** (a) and **2** (b) in D$_2$O (blue filled circle) and DMSO-*d*$_6$ (red filled triangle). R^2 > 0.97 in the linear regression analysis.

Table 2. ^{13}C Spin-lattice relaxation times and chemical exchange rates measured by ^{13}C ST experiments. K_{eq} refers to *trans*/*cis* at the θ_2 torsion angle.

Compound	Solvent	T /°C	K_{eq}	$T_{1,trans}$/s	$k_{trans \to cis}$ /s	$k_{cis \to trans}$[d] /s
1$_{C1'}$	DMSO-d_6	80	2.85[a]	1.85	1.45	4.12
		75	2.93[a]	1.61	0.948	2.78
		65	3.01[a]	1.33	0.429	1.29
		60	3.11[a]	1.22	0.219	0.682
		55	3.21[a]	1.08	0.135	0.434
2$_{C1'}$	DMSO-d_6	80	38.2[b]	8.34	1.52	58.1
		75	40.0[b]	8.18	1.19	47.7
		65	44.1[c]	6.70	0.550	24.3
		60	46.1[c]	2.36	0.324	15.0
		55	48.8[c]	5.58	0.220	10.9
1$_{C1'}$	D$_2$O	80	3.43[a]	3.32	0.608	2.08
		75	3.45[a]	3.03	0.461	1.59
		65	3.59[a]	2.57	0.225	0.807
		60	3.65[a]	2.36	0.151	0.551
		55	3.75[a]	2.07	0.112	0.422
2$_{C1'}$	D$_2$O	80	31.8[b]	16.5	0.624	19.8
		75	33.7[b]	15.3	0.458	15.4
		65	38.3[c]	13.2	0.211	8.09
		60	39.7[c]	11.8	0.160	6.34
		55	42.5[c]	10.9	0.107	4.57

[a] Measured in a ^{1}H NMR spectrum of **1**.

[b] Extrapolated value from ^{13}C NMR measurements.

[c] Measured in a ^{13}C NMR spectrum **2**$_{C1'}$.

[d] Calculated as $k_{cis \to trans} = K_{eq} \cdot k_{trans \to cis}$.

Table 3. Calculated free energy and its enthalpy and entropy contribution at 298 K (kcal·mol^{-1}) for the *trans* vs. *cis* conformational states at the θ_2 torsion angle of compounds **1** and **2** in DMSO-d_6 and D$_2$O as solvents based on a van't Hoff analysis.

Compound	Solvent	ΔG^0	ΔH^0	$-T\Delta S^0$
1	DMSO-d_6	−0.78	−1.04	0.26
2	DMSO-d_6	−2.51	−2.25	−0.26
1	D$_2$O	−0.85	−0.83	−0.02
2	D$_2$O	−2.49	−2.83	0.34

The orientation of the formyl side-chain in **1**^{trans} was also investigated by a ^{1}H,^{1}H-NOESY experiment. Cross-relaxation rates are presented in Table 4. Effective atom-atom distances were calculated for proton spin-pairs related to the formyl side-chain using the isolated spin-pair

approximation[40] and the H3-H4 interaction as the reference distance. The calculated distances are compared to models having different conformations with respect to θ_1 and θ_2. Low RMSDs were observed for the θ_1/θ_2 torsion angles in the region 180°/180° (Figure 6), in overall agreement with the J-based analysis presented above. Even just the geometry optimized model of the *ap,trans* conformation of **1** gave a very good agreement to NOE-derived distances.

Table 4. Cross-relaxation rates (s^{-1}) and effective distances calculated from a ^{1}H,^{1}H-NOESY experiment for **1**^{trans} in DMSO-d_6 using a mixing time (τ_{mix}) of 200 ms and the H3-H4 pair as a reference distance from a quantum mechanical geometry optimized model.

Spin pair	σ_{ij} /s^{-1}	r_{ij} /Å	r_{ij}(QM) /Å
H$_N$-H2	0.051	2.49	2.73
H$_N$-H3	0.023	2.84	2.95
H$_N$-H4	0.013	3.12	3.00
H$_N$-H$_{Fo}$	0.098	2.23	2.24
H$_{Fo}$-H3	0.0038	3.83	3.62
H3-H4	0.060	2.42	2.42
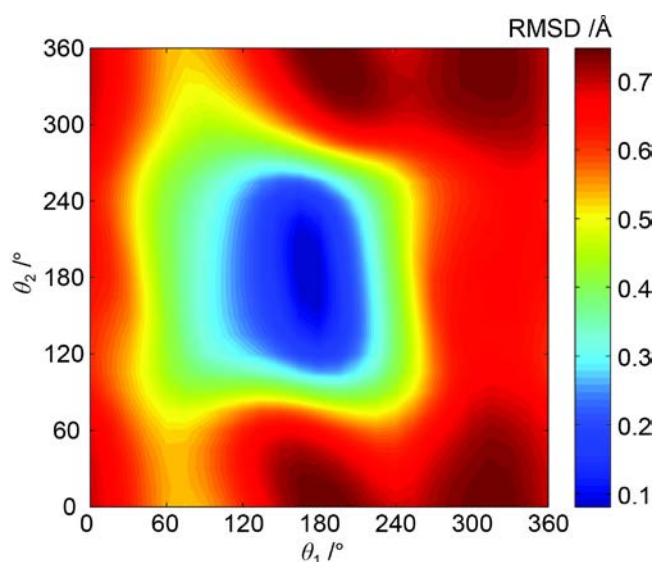
Figure 6. RMSD map of NOE distance (Å) data calculated for different θ_1 and θ_2 torsion angles of **1**^{trans} in DMSO-d_6 based on effective distances of the H2-H$_N$, H3-H$_N$, H4-H$_N$, H$_{Fo}$-H$_N$ and H$_{Fo}$-H3 proton pairs and using the H3-H4 pair as a reference distance.

Dynamic interpretation of the θ_1 torsion angle. Molecular dynamics simulations of *N*-acetyl-D-glucosamine in solution indicate that the θ_1 torsion angle is flexible on a time scale much faster than that of θ_2.[14,41] It is therefore plausible that the J couplings related to the θ_1 torsion are dynamically averaged over two (or more) conformations. The θ_1-related J couplings were re-examined by fitting populations to three-state models by minimizing the RMSD between calculated and experimental values for **1**^{trans} in DMSO-d_6. A three-state model allowing for HB to OH4 and OH2 was investigated,

15

with the same θ_1 torsion angles as the minima in the energy calculations (60°, 180° and 285°). Minimization gave populations of 0%, 75% and 25%, respectively, and an RMSD of 0.66 Hz. The results differed when considering another model in which $\theta_1 = 60°$ is changed to 140°. Here, a low RMSD of 0.36 Hz was found for populations of 47%, 48% and 5% for $\theta_1 = 140°$, 180° and 285°, respectively. Minimization of a similar model but with the 140° state mirrored to 220° resulted in 0% population for the latter θ_1 torsion angle. Additional three-state models with θ_1 of 140° and 180° were examined; however, the third additional state was never populated to any large extent (always $< 15\%$) so it was concluded that the system is best described by a two-state model of $\theta_1 = 140°$ and 180° in which both states are equally populated. This interpretation is consistent with the NOE-based results where a conformations $< 180°$ also are accessible for the θ_1 torsional angle (cf. Figure 6).

In $\mathbf{1}^{trans}$ a long-range $^4J_{HH} \approx 0.8$ Hz is present between the formyl proton and H3 on the sugar ring (Table 1). It has been suggested that such interaction is due to a W-arrangement[12] related to the two torsion angles and occurring in an *sp,trans* relationship (cf. Figure 2, lower left). To investigate the conformational dependence of the $^4J_{HH}$ coupling constant it was computed using DFT methodology as a function of θ_1 rotation keeping the θ_2 torsion in a *trans* orientation (Figure 7). Notably, for $\theta_1 = 180°$ the long-range $^4J_{HH} = -1.1$ Hz and when $\theta_1 = 0°$ the $^4J_{HH}$ coupling constant is very close to zero, to be compared to the magnitude of the experimental value of 0.8 Hz (sign not determined). Thus, the result from these calculations shows that it is not necessary to invoke a large contribution from the *sp* conformation of the θ_1 torsion angle. Convincingly, based on the *ap* conformation derived from ^3J coupling constants and NOE data the magnitude of the calculated $^4J_{HH}$ value is in very good agreement with that determined experimentally. Furthermore, the corresponding calculations for the minor *cis*-conformer (Figure 7) show that for $\theta_1 = 180°$ the long-range $^4J_{HH} = +0.3$ Hz, in perfect agreement with that determined from experiment (Table 1).
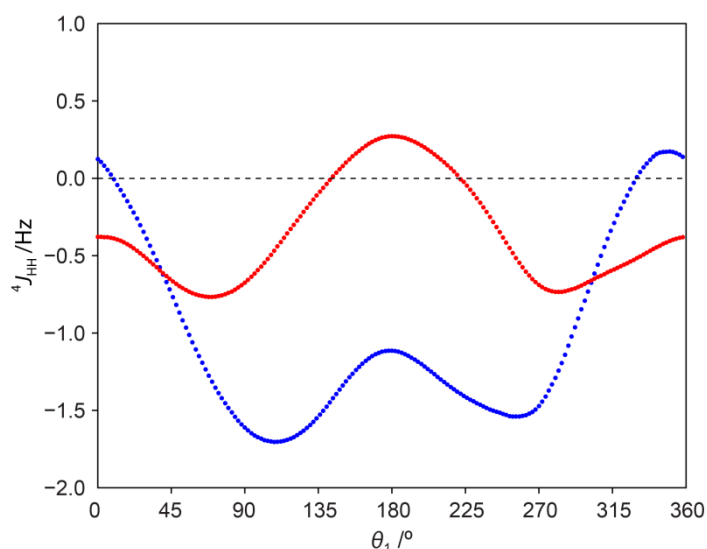
Figure 7. Calculated $^4J_{HH}$ vs. the θ_1 torsion angle in compound **1** keeping the θ_2 torsion in the *trans* orientation (blue) and in the *cis* orientation (red); a conductor-like polarizable continuum model was used for DMSO as solvent.

Exchange kinetics by lineshape analysis. The θ_2 torsion-related chemical exchange between **1**^{trans} and **1**^{cis} is evident when inspecting ^{1}H NMR spectra acquired at high temperature (~100 °C) in DMSO-d_6 as seen in Figure 8.
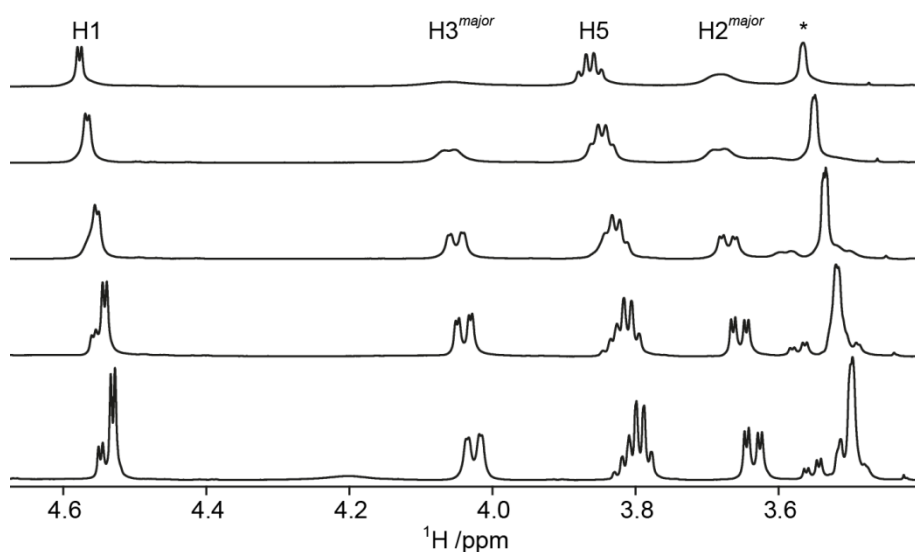
Figure 8. ^{1}H NMR spectra of **1** in DMSO-d_6 at 60, 80, 100, 120 and 140 °C (bottom to top) recorded at 600 MHz, illustrating the coalescence of peaks due to chemical exchange. The asterisk marks the overlapped region of H3^{cis}, H4 and H2^{cis}. NMR spectra were referenced to residual DMSO-d_5 at 2.5 ppm.

At these temperatures the resonances begin to coalesce, a characteristic feature for a system in an intermediate exchange regime. Chemical exchange rates (k_{ex}) can be measured by different NMR

17

spectroscopy techniques, varying depending on chemical exchange regime, and they can be utilized in the calculation of energy barriers for conformational transitions by the construction of Eyring plots. Under intermediate chemical exchange ($\Delta\delta \approx k_{\text{ex}}$), the spectral distortions associated with coalescence make lineshape analysis feasible for the extraction of k_{ex}.[42] Spin-simulations were performed of ^{1}H NMR spectra of **1** in DMSO-d_6 to probe the dynamic behavior at temperatures between 60 °C to 140 °C (Table 5). The k_{ex} extracted by this method is the sum of the transitions between the two sites ($k_{\text{ex}} = k_{A\to B} + k_{B\to A}$),[43] when considering a two-state model $A \rightleftharpoons B$. The individual exchange rate constants can be calculated employing Equation 10, if the equilibrium constant K_{AB} has been determined, e.g., from peak areas or intensities (I) in an NMR spectrum, since $K_{AB} = I_B/I_A = k_{A\to B}/k_{B\to A}$.

$$k_{B\to A} = \frac{k_{\text{ex}}}{1+K_{AB}} \qquad (10)$$

A lineshape analysis was not performed on **2** due to the low abundance of the minor conformer for this compound, which makes spectral distortions less pronounced, and experiments were also not carried out on samples in D_2O because of the lower boiling point of this solvent.

Table 5. Chemical exchange rates (s^{-1}) extracted from lineshape analysis of **1** in DMSO-d_6.

T /°C	k_{ex}/s^{-1}
120	111
110	68.4
100	25.5
90	7.70
80	2.88

Exchange kinetics by ^{13}C saturation transfer. At lower temperatures, under slow exchange ($\Delta\delta \gg k_{\text{ex}}$), the individual chemical exchange rates ($k_{A\to B}$ and $k_{B\to A}$) are directly accessible by the saturation transfer (ST) NMR experiment[26] and by capitalizing on the ^{13}C isotopically labeled compounds **1**$_{C1'}$ and **2**$_{C1'}$ the extraction of k_{ex} is feasible by this method.[10] The experiment relies on a selective saturation of a resonance, in this case that of C1', in conformer *B* and on employing varied saturation times (τ). The reduction of peak intensity of the corresponding resonance in conformer *A* is monitored and $k_{A\to B}$ can be fitted to the data by employing Equation 11, in which R_1 is the longitudinal relaxation rate constant ($R_1 = 1/T_1$).[10,26]

$$M_z^A(\tau) = M_z^A(0) \left(\frac{k_{A\to B}}{k_{A\to B}+R_1^A} \exp\left(-\tau(k_{A\to B} + R_1^A)\right) + \frac{R_1^A}{k_{A\to B}+R_1^A} \right) \qquad (11)$$

[13]C ST experiments were performed on **1**$_{C1'}$ and **2**$_{C1'}$ in D_2O and in DMSO-d_6 and fast inversion recovery experiments were performed to obtain T_1 relaxation times. The experimental data and fits

for the *trans* → *cis* transition at the θ_2 torsion angle upon saturation of the C1' resonance in $1^{cis}_{C1'}$ is presented in Figure 9. Equilibrium constants, calculated from integral ratios of the formyl proton in **1** and C1' intensity ratios measured in ^{13}C NMR spectra (acquired without NOE enhancement) in $2_{C1'}$ are presented in Table 2 together with the chemical exchange rates, acquired with the ^{13}C ST experiment, and measured T_1 relaxation times.
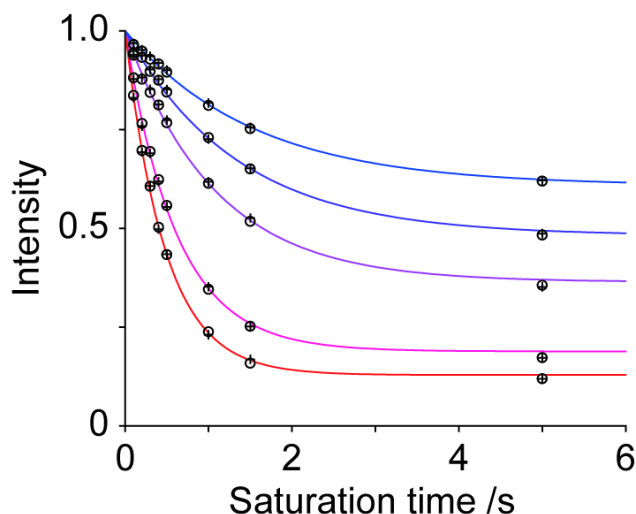
**Figure 9**. The intensity decay of the major C1' peak in ^{13}C NMR ST experiments performed on $1_{C1'}$ in D₂O at 55, 60, 65, 75 and 80 °C (top to bottom); duplicate experiments were performed and experimental data points are represented by o and + signs.

Calculation of transition state energy barriers from NMR data. We started to evaluate the obtained chemical exchange rates for **1** in DMSO-d_6, since this compound has the largest amount of data in this study, by relying on the Eyring equation:[44]

$$k_{ex} = \frac{k_B T}{h} e^{-\Delta G^{\ddagger}/RT} \qquad (12)$$

Analysis of $\ln\left(k_{ex}h/Tk_B\right)$ vs. $1/T$ in an Eyring plot[44] constructed from both lineshape analysis and ^{13}C ST data is presented in Figure 10a. Data were fitted separately for each set and also combined and it is clear that the data from the lineshape analyses is of somewhat lower precision than from the ^{13}C ST experiments. The ^{1}H lineshape analysis is a less appropriate method for the extraction of quantitative data,[44] since accurate estimation of line broadening can be difficult and the high degree of variable parameters can lead to a situation in which a forced fitting of data occurs. These factors are less explicit at coalescence where the spectral distortions are more distinct, which makes accurate estimations feasible. This is reflected in Figure 10a where k_{ex} at 100 °C ($1/T = 2.68 \cdot 10^{-3}$), which was extracted from coalescing resonances, gave best agreement with ^{13}C ST data. Thus, the lineshape analysis data was not included in the subsequent calculation of energy barriers as it did not improve

the fit, which was of excellent quality (with $R^2 > 0.98$) when solely using data from ^{13}C ST experiments with DMSO-d_6 as solvent (Figure 10b); the corresponding ST data for the D$_2$O preparations are presented in Figure 10c.
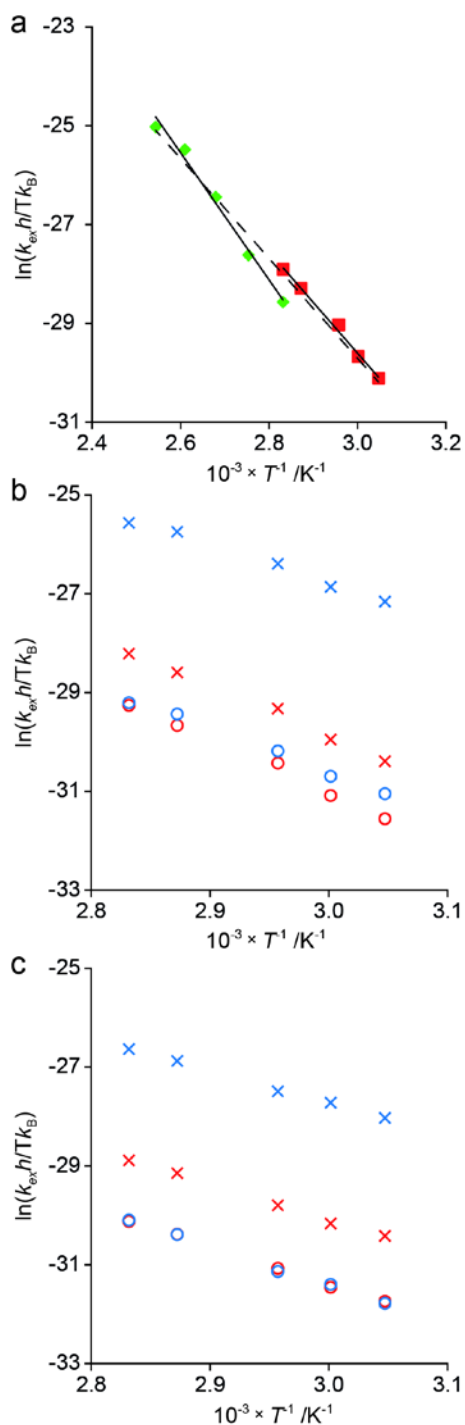
Figure 10. (a) Eyring plot of the line-shape analysis data of **1** in DMSO-d_6 (green) and ^{13}C ST data of **1**$_{C1'}$ in DMSO-d_6 (red, calculated employing $k_{ex} = k_{A \to B} + k_{B \to A}$). Lines show the linear regressions of lineshape analysis (green), ^{13}C ST (red) and both data sets (black dashed). (b and c) Eyring plots of measured $k_{trans \to cis}$ (circles) and calculated $k_{cis \to trans}$ (crosses) employing ^{13}C NMR ST experiments for **1**$_{C1'}$ (red) and **2**$_{C1'}$ (blue) in DMSO-d_6 (b) and in D$_2$O (c).

20

Transition enthalpies ($\Delta H^{\ddagger}$) and entropies ($\Delta S^{\ddagger}$) can be extracted from the slopes and intercepts of Eyring plots,[45] respectively. These data are presented in Table 6 together with calculated free energies of activation at room temperature ($\Delta G^{\ddagger}_{298}$). The uneven conformational equilibria observed by NMR spectroscopy for **1** and **2** are reflected in a lower $\Delta G^{\ddagger}_{298}$ of ~0.8 and 2.5 kcal·mol^{-1}, respectively, for the *cis→trans* transition. On the other hand, for the *trans→cis* transitions all calculated $\Delta G^{\ddagger}_{298}$ are ~20 kcal·mol^{-1}. These $\Delta G^{\ddagger}$ are similar to the results obtained for *N*-formyl- and *N*-acetylglucosamines described by Hu et al.[10] as well as for other amides.[37,46] Some trends can also be distinguished from the thermodynamic data. The major contribution to the transition state barriers comes from the enthalpic term $\Delta H^{\ddagger}$. In addition, the enthalpy contributions are lower and the entropy contributions are stronger for energy barriers in D$_2$O. This observation may be explained by a stabilization of the transition state by a hydrogen bond donation from a solvent molecule in D$_2$O, which is not possible in the aprotic DMSO-*d*$_6$. A hydrogen bond between the carbonyl oxygen and a solvent molecule in the transition state would lower the enthalpy but at the same time be entropically unfavored due to the structuring of solvent. In DMSO-*d*$_6$, the importance of the enthalpic component to $\Delta G^{\ddagger}$ increases, and whereas the entropic term $-T\Delta S^{\ddagger}$ is still present in **2** it is absent or minor in **1**.

Table 6. Calculated transition state energy barriers (kcal·mol^{-1}) with standard deviation in parenthesis.

Compound	Solvent	Transition	$\Delta G^{\ddagger}_{298}$	$\Delta H^{\ddagger}$	$-T\Delta S^{\ddagger}_{298}$
1$_{C1'}$	DMSO-*d*$_6$	*trans→cis*	20.6(1.3)	21.2(1.0)	−0.6(0.8)
		cis→trans	19.8(1.2)	20.1(0.9)	−0.3(0.8)
2$_{C1'}$	DMSO-*d*$_6$	*trans→cis*	20.0(1.1)	17.5(0.8)	2.5(0.7)
		cis→trans	17.5(1.1)	15.3(0.8)	2.2(0.7)
1$_{C1'}$	D$_2$O	*trans→cis*	20.2(0.5)	15.3(0.4)	4.9(0.4)
		cis→trans	19.3(0.6)	14.4(0.4)	4.9(0.4)
2$_{C1'}$	D$_2$O	*trans→cis*	20.3(0.6)	15.6(0.4)	4.7(0.4)
		cis→trans	17.8(0.4)	12.9(0.3)	4.9(0.3)

CONCLUSIONS

The experimental data presented in this study confirm that the amide side-chains of **1** and **2** primarily adopt an *ap,trans* arrangement; however, the slow rotation around the amide bond results in an *ap,cis* conformer present with population ratios of ~4 for the former compound and ~80 for the latter at room temperature in D$_2$O, the structural difference being the replacement of the small hydrogen atom in the *N*-formyl group with the significantly larger methyl group in the *N*-acetyl substituent. Intramolecular hydrogen bonds between the amide oxygen and either OH4 or OH2 observed in QM energy calculations of the compounds could not be experimentally confirmed to occur to any major extent. This could be due to competition with solvent molecules which are able to accept hydrogen bonds and this is not accounted for in the QM calculations. Altogether, energy calculations, *J*

couplings and NOE-based analysis indicate that the *ap,trans* conformation is favored in **1**, with a slight tilt where $\theta_1 < 180°$, and this behavior was also observed for **2**.

Energy calculations with restricted hydrogen bonding indicate that the conformation is only marginally solvent dependent for the solvents used herein. This is also supported by the fact that the measured *J* couplings are similar between corresponding conformations in each solvent. The energy barriers for the rotation around the amide bond measured in this study are similar to the ones previously measured for *N*-acylated D-glucosamine compounds. The lower transition enthalpies and higher entropy penalties observed by experiments in D_2O imply that the transition state can be stabilized by a hydrogen bond in this solvent.

ACKNOWLEDGEMENTS

Supporting information. $^1H,^1H$-NOESY spectrum of compound **1**, ^1H and ^{13}C NMR spectra of synthesized compounds, Cartesian coordinates for 360 geometry optimized structures of compound **1** and the *ap,trans* geometry optimized model of compound **1** in pdb-format.

REFERENCES

(1) Lindberg, B.; Lindqvist, B.; Lönngren, J.; Powell, D. A. Structural Studies of the Capsular Polysaccharide from Streptococcus Pneumoniae Type 1. *Carbohydr. Res.* **1980**, *78*, 111–117.

(2) Kenne, L.; Lindberg, B.; Petersson, K.; Katzenellenbogen, E.; Romanowska, E. Structural Studies of the O-Specific Side-Chains of the Shigella Sonnei Phase I Lipopolysaccharide. *Carbohydr. Res.* **1980**, *78*, 119–126.

(3) Vinogradov, E.; Peppler, M. S.; Perry, M. B. The Structure of the Nonreducing Terminal Groups in the O-Specific Polysaccharides from Two Strains of Bordetella Bronchiseptica. *Eur. J. Biochem.* **2000**, *267*, 7230–7236.

(4) Zaccheus, M. V.; Ali, T.; Cloeckaert, A.; Zygmunt, M. S.; Weintraub, A.; Iriarte, M.; Moriyón, I.; Widmalm, G. The Epitopic and Structural Characterization of Brucella Suis Biovar 2 O-Polysaccharide Demonstrates the Existence of a New M-Negative C-Negative Smooth Brucella Serovar. *PLoS One* **2013**, *8*, e53941.

(5) Shashkov, A. S.; Arbatsky, N. P.; Widmalm, G.; Knirel, Y. A.; Zych, K.; Sidorczyk, Z. Structure and Cross-Reactivity of the O-Specific Polysaccharide of Proteus Penneri Strain 26, Another Neutral Proteus O-Antigen Containing 2- Acetamido-2,6-Dideoxy-L-Glucose (N-Acetyl-L-Qninovosamine). *Eur. J. Biochem.* **1998**, *253*, 730–733.

(6) Jonsson, K. H. M.; Weintraub, A.; Widmalm, G. Structural Determination of the O-Antigenic Polysaccharide from Escherichia Coli O74. *Carbohydr. Res.* **2009**, *344*, 1592–1595.

(7) Kenne, L.; Lindberg, B.; Unger, P.; Gustafsson, B.; Holme, T. Structural Studies of the Vibrio Cholera O-Antigen. *Carbohydr. Res.* **1982**, *100*, 341–349.

(8) Yokota, S.; Kaya, S.; Araki, Y.; Ito, E. Structure of the O-Polysaccharide Chain of Lipopolysaccharide from Pseudomonas Aeruginosa IID 1001 (ATCC 27577). *J. Biochem.*

1988, *104*, 671–678.

(9)   Mobli, M.; Almond, A. N-Acetylated Amino Sugars: The Dependence of NMR 3J(HNH2)-Couplings on Conformation, Dynamics and Solvent. *Org. Biomol. Chem.* **2007**, *5*, 2243–2251.

(10)   Hu, X.; Zhang, W.; Carmichael, I.; Serianni, A. S. Amide Cis-Trans Isomerization in Aqueous Solutions of Methyl N-Formyl-D-Glucosaminides and Methyl N-Acetyl-D-Glucosaminides: Chemical Equilibria and Exchange Kinetics. *J. Am. Chem. Soc.* **2010**, *132*, 4641–4652.

(11)   Ganesh, N. V.; Sadowska, J. M.; Sarkar, S.; Howells, L.; McGiven, J.; Bundle, D. R. Molecular Recognition of Brucella A and M Antigens Dissected by Synthetic Oligosaccharide Glycoconjugates Leads to a Disaccharide Diagnostic for Brucellosis. *J. Am. Chem. Soc.* **2014**, *136*, 16260–16269.

(12)   Kenne, L.; Unger, P.; Wehler, T. Synthesis and Nuclear Magnetic Resonance Studies of Some N-Acylated Methyl 4-Amino-4,6-Dideoxy-Alfa-D-Mannopyranoside. *J. Chem. Soc., Perkin Trans. 1* **1988**, 1183–1186.

(13)   Säwén, E.; Stevensson, B.; Östervall, J.; Maliniak, A.; Widmalm, G. Molecular Conformations in the Pentasaccharide LNF-1 Derived from NMR Spectroscopy and Molecular Dynamics Simulations. *J. Phys. Chem. B* **2011**, *115*, 7109–7121.

(14)   Pendrill, R.; Jonsson, K. H. M.; Widmalm, G. Glycan Synthesis , Structure , and Dynamics : A Selection. *Pure Appl. Chem.* **2013**, *85*, 1759–1770.

(15)   Zaccheus, M. V.; Pendrill, R.; Jackson, T. A.; Wang, A.; Auzanneau, F.-I.; Widmalm, G. Conformational Dynamics of a Central Trisaccharide Fragment of the LeaLex Tumor Associated Antigen Studied by NMR Spectroscopy and Molecular Dynamics Simulations. *Eur. J. Org. Chem.* **2012**, 4705–4715.

(16)   Knirel, Y. A.; Kocharova, N. A.; Bystrova, O. V; Katzenellenbogen, E.; Gamian, A. Structures and Serology of the O-Specific Polysaccharides of Bacteria of the Genus Citrobacter. *Arch. Immunol. Ther. Exp. (Warsz).* **2002**, *50*, 379–391.

(17)   Mobarak, H.; Engström, O.; Widmalm, G. Synthesis of Methyl 3-Amino-3,6-Dideoxy-α-D-Galactopyranoside Carrying Different Amide Substituents. *RSC Adv.* **2013**, *3*, 23090–23097.

(18)   De Luca, L.; Giacomelli, G.; Porcheddu, A.; Salaris, M. Amide_synlett_2004. *Synlett* **2004**, 2570–2572.

(19)   Laatikainen, R.; Niemitz, M.; Weber, U.; Sundelin, J.; Hassinen, T.; Vepsäläinen, J. General Strategies for Total-Lineshape-Type Spectral Analysis of NMR Spectra Using Integral-Transform Iterator. *J. Magn. Reson. Ser. A* **1996**, *120*, 1–10.

(20)   del Río-Portilla, F.; Blechta, V.; Freeman, R. Measurement of Poorly Resolved Splittings by J Doubling in the Frequency Domain. *J. Magn. Reson. Ser. A* **1994**, *111*, 132–135.

(21)   Garza-García, A.; Ponzanelli-Velázquez, G.; del Río-Portilla, F. Deconvolution and Measurement of Spin-Spin Splittings by Modified J Doubling in the Frequency Domain. *J. Magn. Reson.* **2001**, *148*, 214–219.

(22)   Meissner, A.; Sørensen, O. W. Measurement of J(H,H) and Long-Range J(X,H) Coupling Constants in Small Molecules. Broadband XLOC and J-HMBC. *Magn. Reson. Chem.* **2001**, *39*, 49–52.

(23)   Thrippleton, M. J.; Keeler, J. Elimination of Zero-Quantum Interference in Two-Dimensional NMR Spectra. *Angew. Chemie - Int. Ed.* **2003**, *42*, 3938–3941.

(24)   Dixon, A. M.; Widmalm, G.; Bull, T. E. Modified GOESY in the Analysis of Disaccharide Conformation. *J. Magn. Reson.* **2000**, *147*, 266–272.

(25) Canet, D.; Levy, G. C.; Peat, I. R. Time Saving in 13C Spin-Lattice Relaxation Measurements by Inversion-Recovery. *J. Magn. Reson.* **1975**, *18*, 199–204.

(26) Forsén, S.; Hoffman, R. Study of Moderatly Rapid Chamical Exchange Reactions by Means of Nuclear Magnetic Double Resonance. *J. Chem. Phys.* **1963**, *39*, 2892–2901.

(27) Hu, X.; Carmichael, I.; Serianni, A. S. N -Acetyl Side-Chains in Saccharides: NMR J - Coupling Equations Sensitive to CH-NH and NH-CO Bond Conformations in 2-Acetamido- 2-Deoxy-Aldohexopyranosyl Rings. *J. Org. Chem.* **2010**, *75*, 4899–4910.

(28) Ludvigsen, S.; Andersen, K. V; Poulsen, F. M. Accurate Measurements of Coupling Constants from Two-Dimensional Nuclear Magnetic Resonance Spectra of Proteins and Determination of Phi-Angles. *J. Mol. Biol.* **1991**, *217*, 731–736.

(29) Kao, L.-F.; Barfield, M. Conformational Dependencies of Vicinal 13C (0) -N-C , - â€™ H Coupling Constants in Compounds Which Model the Peptide Backbone. *J. Am. Chem. Soc.* **1985**, *107*, 2323–2330.

(30) Frisch, M. J.; Trucks, G. W.; Schlegel, H. B.; Scuseria, G. E.; Robb, M. A.; Cheeseman, J. R.; Scalmani, G.; Barone, V.; Petersson, G. A.; Nakatsuji, H.; et al. *Gaussian 09, Revision D.01*; Gaussian, Inc.: Wallington CT, 2016.

(31) Barone, V.; Cossi, M. Conductor Solvent Model. *J. Phys. Chem. A* **2001**, *102*, 1995–2001.

(32) Cossi, M.; Rega, N.; Scalmani, G.; Barone, V. Energies, Structures, and Electronic Properties of Molecules in Solution with the C-PCM Solvation Model. *J. Comput. Chem.* **2003**, *24*, 669–681.

(33) Wolinski, K.; Hinton, J. F.; Pulay, P. Efficient Implementation of the Gauge-Independent Atomic Orbital Method for NMR Chemical Shift Calculations. *J. Am. Chem. Soc.* **1990**, *112*, 8251–8260.

(34) Cheeseman, J. R.; Trucks, G. W.; Keith, T. A.; Frisch, M. J. A Comparison of Models for Calculating Nuclear Magnetic Resonance Shielding Tensors. *J. Chem. Phys.* **1996**, *104*, 5497–5509.

(35) Becke, A. D. Density-Functional Thermochemistry. III. The Role of Exact Exchange. *J. Chem. Phys.* **1993**, *98*, 5648–5652.

(36) Deng, W.; Cheeseman, J. R.; Frisch, M. J. Calculation of Nuclear Spin - Spin Coupling Constants of Molecules with First and Second Row Atoms in Study of Basis Set Dependence. *J. Chem. Theory Comput.* **2006**, *2*, 1028–1037.

(37) Wiberg, K. B. The Interaction of Carbonyl Groups with Substituents. *Acc. Chem. Res.* **1999**, *32*, 922–929.

(38) Cagas, P.; Kaluarachchi, K.; Bush, C. A. 2D NOESY Simulations of Amide Protons in Acetamido Sugar. *J. Am. Chem. Soc.* **1991**, *113*, 6815–6822.

(39) Varani, K.; Gessi, S.; Merighi, S.; Borea, P. A. Van't Hoff Based Thermodynamics. In *Thermodynamics and Kinetics of Drug Binding*; Keserü, G. M., Swinney, D. C., Eds.; Wiley-VCH Verlag GmbH & Co. KGaA: Weinheim, Germany, 2015; pp 15–35.

(40) Thomas, P. D.; Basus, V. J.; James, T. L. Protein Solution Structure Determination Using Distances from Two-Dimensional Nuclear Overhauser Effect Experiments: Effect of Approximations on the Accuracy of Derived Structures. *Proc. Natl. Acad. Sci. U. S. A.* **1991**, *88*, 1237–1241.

(41) Zhong, Y.; Bauer, B. A.; Patel, S. Solvation Properties of N-Acetyl-Beta-Glucosamine: Molecular Dynamics Study Incorporating Electrostatic Polarization. *J. Comput. Chem.* **2011**, *32*, 3339–3353.

(42) Rönnols, J.; Manner, S.; Ellervik, U.; Widmalm, G. Conformational Effects due to

Stereochemistry and C3-Substituents in Xylopyranoside Derivatives as Studied by NMR Spectroscopy. *Org. Biomol. Chem.* **2014**, *12*, 8031–8035.

(43) Kowalewski, J.; Mäler, L. *Nuclear Spin Relaxation in Liquids: Theory, Experiments, and Applications*; Taylor & Francis: Boca Raton, FL, 2006.

(44) Bain, A. D. Chemical Exchange in NMR. *Prog. Nucl. Magn. Reson. Spectrosc.* **2003**, *43*, 63–103.

(45) Lente, G.; Fábián, I.; Poë, A. J. A Common Misconception about the Eyring Equation. *New J. Chem.* **2005**, *29*, 759–760.

(46) Dugave, C.; Demange, L. Cis-Trans Isomerization of Organic Molecules and Biomolecules: Implications and Applications. *Chem. Rev.* **2003**, *103*, 2475–2532.